iScience

CellPress
OPEN ACCESS

Article

Hydrogen evolution catalysis by terminal molybdenum-oxo complexes

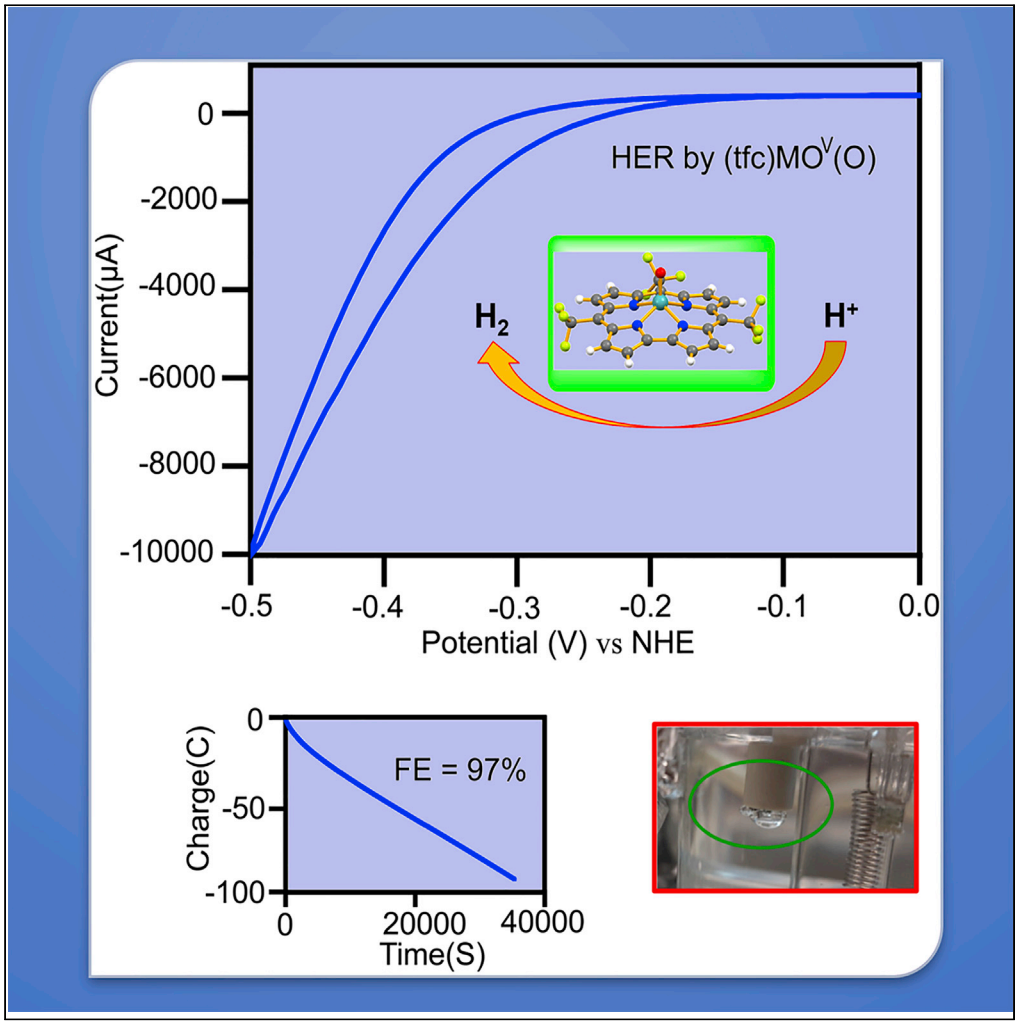

Pinky Yadav, Izana Nigel-Etinger, Amit Kumar, ..., Sophia Lipstman, Israel Goldberg, Zeev Gross

chr10zg@technion.ac.il

Highlights

Full characterization of (oxo)molybdenum(V) corroles with desired redox properties

Mechanism of action studies of homogeneous HER catalysis thereby

Introduction of durable (oxo)molybdenum-modified carbon electrodes

Heterogeneous HER at low overpotentials and with very large Faradaic yields

Yadav et al., iScience 24, 102924
August 20, 2021
https://doi.org/10.1016/j.isci.2021.102924

iScience

CellPress
OPEN ACCESS

Article

Hydrogen evolution catalysis by terminal molybdenum-oxo complexes

Pinky Yadav,[1,4] Izana Nigel-Etinger,[1,4] Amit Kumar,[1,4] Amir Mizrahi,[1,3] Atif Mahammed,[1] Natalia Fridman,[1] Sophia Lipstman,[2] Israel Goldberg,[2] and Zeev Gross[1,5,*]

SUMMARY

Stable complexes with terminal triply bound metal-oxygen bonds are usually not considered as valuable catalysts for the hydrogen evolution reaction (HER). We now report the preparation of three conceptually different (oxo)molybdenum(V) corroles for testing if proton-assisted 2-electron reduction will lead to hyper-reactive molybdenum(III) capable of converting protons to hydrogen gas. The upto 670 mV differences in the $[(oxo)Mo(IV)]^{-}/[(oxo)Mo(III)]^{-2}$ redox potentials of the dissolved complexes came into effect by the catalytic onset potential for proton reduction thereby, significantly earlier than their reduction process in the absence of acids, but the two more promising complexes were not stable at practical conditions. Under heterogeneous conditions, the smallest and most electron-withdrawing catalyst did excel by all relevant criteria, including a 97% Faradaic efficiency for catalyzing HER from acidic water. This suggests complexes based on molybdenum, the only sustainable heavy transition metal, as catalysts for other yet unexplored green-energy-relevant processes.

INTRODUCTION

The non-sustainability of platinum, by far the best catalyst for reduction of protons to hydrogen (the hydrogen evolution reaction [HER]), and also inspiration from biology (e.g., Fe-hydrogenases) continues to drive focus on developing catalysts based on cheap, non-toxic, and earth-abundant metal complexes (Abbas and Bang, 2015; Bullock et al., 2014; Fukuzumi et al., 2018; Guo et al., 2020; Mondal et al., 2013; Roger et al., 2017; Xie et al., 2020). Molybdenum may safely be considered the only non-precious heavy transition metal, and it is also essential for human life due to its presence and roles in more than 30 enzymes (e.g., DMSO reductase, sulfite oxidase, xanthine oxidase) (Schwarz et al., 2009). These participate in both oxidation (of sulfur containing compounds) and reduction processes (e.g., nitrogen to ammonia by nitrogenases) (Spence, 1980); and there are also human diseases that are related to this essential metal (molybdenum cofactor deficiency) (Chatzistathis, 2014). The shortlist of efforts devoted to using synthetic molybdenum complexes as catalysts is not limited to enzyme-mimicking studies such as oxidation of sulfides and sulfoxides by H_2O_2 (Carrasco et al., 2018; Thiruvengetam and Chand, 2018) and the reduction of nitrogen to ammonia (Weare et al., 2006; Wickramasinghe et al., 2017) but also processes like the electrocatalytic HER that is of prime importance for hydrogen economy (Benck et al., 2014; Hua et al., 2020; Xiao et al., 2014).

The important chemistry of molybdenum complexes remains a main motivation for investigating its chemistry within the trianionic N_4-coordination sphere of corroles, well known to increase the activity of low valent metal ions chelated by it (Johansen et al., 2011; Mody et al., 2009; Nayak et al., 2020; Sashuk et al., 2004). Regardless of the molybdenum source used, metalation of corroles invariably leads to isolation of robust 5-coordinated (oxo)molybdenum(V) complexes. The terminal molybdenum-oxygen moiety in the axial position is very inert due to the triple bond connecting the elements, and transformation into isolable molybdenum(IV) complexes requires the combination of very strong reducing agents and highly electrophilic additives. The terminal oxo ligand affords a high inertness at the opposite axial position (Nigel-Etinger et al., 2013)(Schweyen et al., 2017). To the best of our knowledge, all attempted efforts for the isolation of molybdenum(III) corroles were not successful (Alemayehu et al., 2017; Buckley and Arnold, 2015).

We have now turned to halogenation of the β-pyrrole-C atoms of $(tpfc)Mo^{V}(O)$ [tpfc = the trianion of 5,10,15-tris(pentafluorophenyl)corrole] (Chart 1), anticipating that this will lead to dramatic changes in the spectroscopic, electrochemical, and catalytic properties. Guided by recent results with other

[1]Schulich Faculty of Chemistry, Technion - Israel Institute of Technology, Haifa, Israel

[2]School of Chemistry, Sackler Faculty of Exact Sciences, Tel Aviv University, Tel Aviv 6997801, Israel

[3]Chemistry Department, Nuclear Research Centre Negev, Beer Sheva 84190, Israel

[4]These authors contributed equally

[5]Lead contact

*Correspondence: chr10zg@technion.ac.il

https://doi.org/10.1016/j.isci.2021.102924

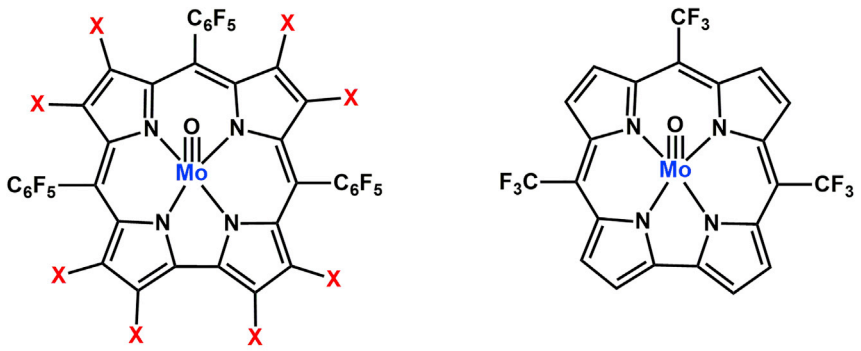

(tpfc)Mo^{V}(O): X = H
(tpfc-Br_8)Mo^{V}(O): X = Br
(tpfc-Cl_8)Mo^{V}(O): X = Cl

(tfc)Mo^{V}(O)

Chart 1. Chemical structures of the investigated (oxo)molybdenum(V) corroles

metallocorroles, which disclosed *meso*-CF_3 to be more effective than *meso*-C_6F_5 substituents for shifting the redox potentials in the desired direction (Chen et al., 2018; Sudhakar et al., 2017), we have also prepared and studied (tfc)Mo^{V}(O) [tfc = the trianion of 5,10,15-tris(trifluoromethyl)corrole] (Chart 1). All new complexes were fully characterized, and their spectroscopic, electrochemical, and HER catalyzing properties are compared relative to the previously reported (tpfc)Mo^{V}(O) complex (Luobeznova et al., 2006).

RESULTS AND DISCUSSION

Synthesis and characterization of (oxo)molybdenum(V) corroles

Envisioning that halogenation of the macrocyclic CH bonds could provide more reducible complexes, direct chlorination of (tpfc)Mo^{V}(O) was carried out by treating it with excess chlorine in benzene solution, following a previously reported procedure on different metallocorroles (Mahammed et al., 2012). The isolated complex was crystallized and subjected to X-ray diffraction analysis, which revealed that chlorination did not proceed to completion. In the refined structural model, the Cl atoms were found to be partitioned between the eight β-sites, accounting altogether for nearly six Cl atoms per corrole (Figure 1A). This is true for both crystallographically independent molecules of the asymmetric unit. Further support was obtained from mass spectroscopy analysis which also revealed only six chlorine atoms on the corrole ligand for the most intense cluster of signals (Figure S5). Similar results were obtained from bromination of (tpfc)Mo^{V}(O) with either bromine or NBS, which for other metal complexes of the same corrole induce clean octa-bromination (Mahammed et al., 2011). Although only an approximate structural model could be obtained from the severely twinned crystals obtained in this case, crystallographic refinement of the bromine substituents suggested partitioning of seven Br atoms between the eight β-carbons of the corrole ring.

Since direct halogenation on the molybdenum corrole was not fully effective, a different method was implemented as to achieve better results: insertion of an acid-labile metal (only manganese and copper are relevant in the case of corroles), bromination, demetalation, and molybdenum insertion. The adopted starting point was the preparation of (tpfc)Mn^{III} (Gross et al., 2000), followed by the bromination of all its β-pyrrole positions (Golubkov et al., 2001), and subsequent demetalation by sulfuric acid (Mandoj et al., 2008). Molybdenum was inserted to the such formed free base H_3(tpfc-Br_8) ligand by the use of (cyclopentadienyl)Mo^{V} tetrachloride and refluxing the reaction mixture for 40 min under N_2 in decalin solution. The successfully crystallized molybdenum complex was proven to be the fully brominated (tpfc-Br_8)Mo^{V}(O) indeed (Figure 1B). The characteristics of the halogenated macrocycles are significantly red-shifted absorption maxima (Figures S6 and S7): (tpfc)Mo^{V}(O) is characterized with a Soret band at 430 nm, while the λ_{max} of the chlorinated and brominated complexes is 440 nm and 450 nm, respectively (Figures S7).

For the earlier outlined reasons, the (oxo)molybdenum complex (tfc)Mo^{V}(O) with CF_3 rather than C_6F_5 groups on the three *meso*-C atoms of the macrocycle was prepared by heating 5,10,15-tris(trifluoromethyl)corrole H_3(tfc) (Yadav et al., 2020) and $Mo(CO)_6$ in decalin at 170°C. Examination of (tfc)Mo^{V}(O) by X-ray crystallography revealed that the central metal ion protrudes from the mean plane by 0.914 Å and also

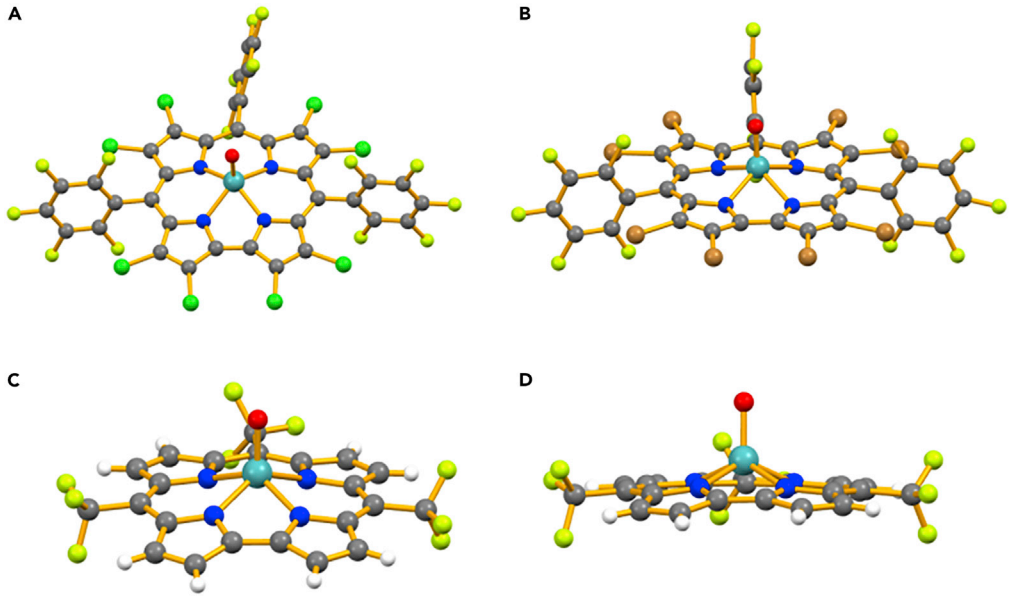

Figure 1. Single crystal X-ray structures of (oxo)molybdenum(V) corroles

(A) View of the two crystallographically independent molecules in the crystal structure of (tpfc-Cl_6)Mo^V(O), showing the approximate partitioning of the Cl-substituents among the eight β-positions of the corrole rings.

(B) Projection of the molecular structure in the crystal of (tpfc-Br_8)Mo^V(O). All Br-atoms are in full occupancy.

(C and D) (C) Front and (D) side view of (tfc)Mo^V(O) single crystal X-ray structure.

an M-O bond length of 1.676 Å (Figures 1C and 1D). Both values are larger than for (tpfc-Br_8)Mo^V(O) and (tpfc-Cl_6)Mo^V(O), wherein the Mo(O) centers are 0.708 and 0.839 Å above the 23-atom mean plane and the Mo-O bond lengths are 1.647 and 1.666 Å, respectively.

Cyclic voltammetry

Cyclic voltammograms were recorded for (tpfc)Mo^V(O), (tfc)Mo^V(O), and (tpfc-Br_8)Mo^V(O), in N,N-dimethylformamide (DMF) under N_2 atmosphere (Figure 2), for elucidating the electronic effect of the *meso*-C and β-pyrrole substituents. All three (oxo) Mo complexes exhibit two reversible redox processes located in the range of −1.5 to 0.5 V. The redox processes of (tpfc)Mo^V(O) with half-wave potentials ($E_{1/2}$) of −0.17 V and −1.45 V correspond to Mo(IV)/Mo(V) and Mo(III)/Mo(IV) couples, respectively. For (tfc)Mo(O), these processes are positively shifted by 210 mV and 250 mV: $E_{1/2}(1)$ = 0.04 and $E_{1/2}(2)$ = −1.20 V. These anodic shifts testify for a stronger electron withdrawing effect by *meso*-CF_3 relative to *meso*-C_6F_5 groups. Bromination of the β-pyrrole C atoms had an even stronger impact, with the $E_{1/2}(1)$ = 0.32 V and $E_{1/2}(2)$ = −0.78 V for (tpfc-Br_8)Mo^V(O) reflecting positive shifts of 490 mV for the Mo(IV)/Mo(V) and 670 mV for the Mo(III)/Mo(IV) processes relative to (tpfc)Mo(O). These values may also be presented as 60-82 mV/Br atom positive shifts in redox potentials, much higher than what is achievable for analogous porphyrin complexes. This adds confidence to the analysis reported in previous work (Bhyrappa et al., 2003; Mahammed et al., 2011), where the different responses to Br-substitution on the macrocyclic periphery of corroles and porphyrins were noticed and analyzed. The X-ray structures of β-pyrrole-brominated corroles/porphyrins revealed that bromine-induced distortions of the macrocycle are much more pronounced for porphyrins than for corroles. This is one main factor that leads to a significant attenuation of the expected effect of bromination on redox potentials of metal ions chelated by porphyrins relative to corroles (Mahammed et al., 2011). The last aspect of emphasis is that only (tfc)Mo^V(O) exhibits another clear reduction process at −1.69 V that may be tentatively assigned to a Mo(II)/Mo(III) couple (Figures S15). Despite of expectation of obtaining this for (tpfc-Br_8)Mo^V(O) as well and at even less negative potentials, it was much less well behaved than for (tfc)Mo^V(O). This testifies for some irreversible decompositions, likely due to the instability of C-Br bonds at very negative potentials.

Homogeneous HER electrocatalysis

Having demonstrated the facile access to low valent molybdenum metallocorroles, it attracts the interest to explore their interactions with small molecules and possible catalytic activation thereof. Effective hydrogen

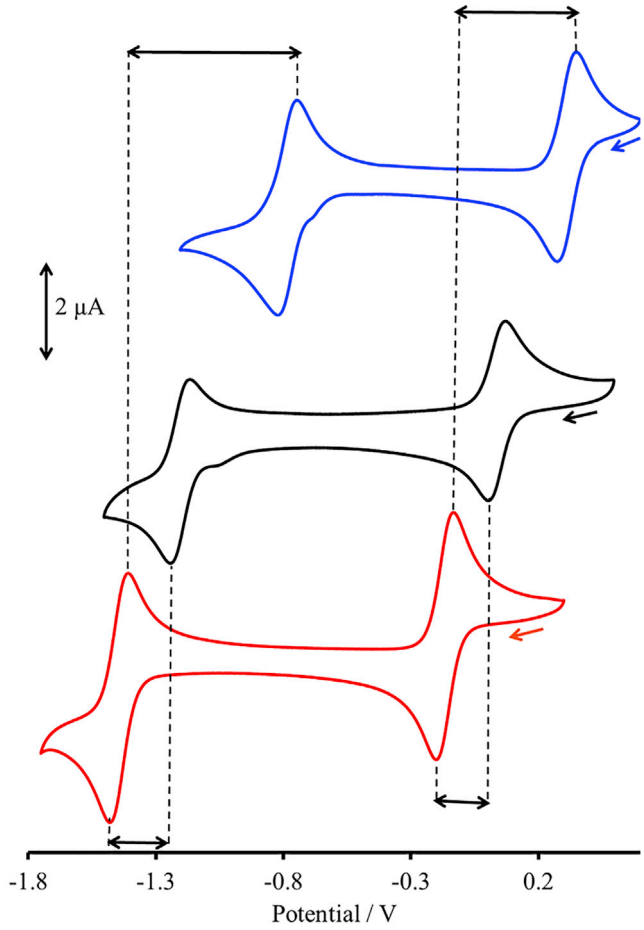

Figure 2. Cyclic voltammograms of (oxo)molybdenum(V) corroles

Cyclic voltammograms of (tpfc)Mo^{V}(O), (tfc)Mo^{V}(O), and (tpfc-Br_8)Mo^{V}(O) (red, black, and blue traces, respectively; 1 mM) recorded in N_2-purged DMF solution of TBAP (0.1 M) on a glassy carbon electrode at 80 mV/s. The reference electrode was Ag/AgCl.

evaluation reaction (HER) from trifluoroacetic acid, acetic acid, acetonitrile/water, and neutral buffer solution solutions were recently reported by employing Fe^{IV}, Co^{III}, and Cu^{III} corroles as electrocatalysts (Chen et al., 2020; Lei et al., 2014, 2015; Lin et al., 2020; Mahammed et al., 2014; Sudhakar et al., 2020; Sun et al., 2017; Zhong et al., 2019). On the other hand, there are no reports regarding HER catalysis by any (oxo)metal porphyrins or corroles despite of their rich redox chemistry. We have hence first tested the electrocatalytic proton reduction using protonated DMF (DMF-H^+) as the proton source in the presence of 1 mM (tpfc)Mo^{V}(O) as the electrocatalyst (Figure 3). Incremental increase in current and formation of irreversible reduction waves as more acid is added serve as indications for proton reduction; and the involvement of the catalyst is clearly evident by comparison with results obtained in its absence (the dashed lines), as well as by the maximal current obtained close to the Mo(IV)/Mo(III) redox process. Another interesting aspect is that the catalytic current (i_c) precedes the cathodic maximum (i_p) which suggests it be due to a proton-assisted electron transfer process. Most important is to note that the intensity of the Mo^{IV}/Mo^{V} couple remains completely unaffected under all conditions as this testifies for the return of the metal center to its original Mo^{V} state after proton reduction and accordingly for the stability of the catalyst.

The comparison between the three complexes was highly rewarding regarding analysis of the reaction mechanism(s). Both new complexes also catalyzed the HER but with more complex phenomena (Figures S12 and S13). As expected, based on the reduction potentials in the absence of acid, the onset potentials for (tfc)Mo^{V}(O) and (tpfc-Br_8)Mo^{V}(O) are shifted positively compared to (tpfc)Mo^{V}(O). However, two catalytic waves are apparent for both complexes, which is best demonstrated for (tfc)Mo(O): they appear at about

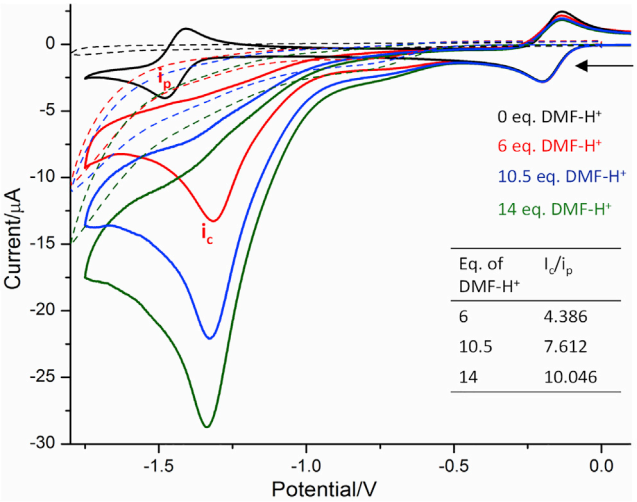

Figure 3. The influence of DMF-H$^+$ on cyclic voltammograms of (tpfc)Mo^V(O)

The above cyclic voltammograms were recorded in a DMF solution of TBAP (tertbutylammonium perchlorate, 0.1 M), on a glassy carbon electrode at 80 mVs^{-1}. Catalyst concentration = 1 mM. Potentials are listed versus Ag/AgCl. Dashed lines represent the influence of DMF-H$^+$ without catalyst.

equal catalytic current at $E_{p,c}$ = −0.94 and −1.38 V at low (6 equivalents) DMF-H$^+$ concentration, while higher acid concentration (29 equivalents) affects mostly the latter process (Figure 4, the blue dashed and full traces, respectively). Common to both (tfc)Mo^V(O) and (tpfc-Br$_8$)Mo^V(O) is that the less and more effective catalytic waves appear earlier and later, respectively, than the Mo(III)/Mo(IV) redox couple in the absence of acid, as demonstrated by the perpendicular lines in Figure 4. Taken together with the results summarized in Table S1, for proton reduction using the three molybdenum complexes at a single DMF-H$^+$ concentration, it clearly shows that (a) replacing C_6F_5 by CF_3 as *meso*-C substituents or bromination of the β-pyrrole carbon atoms leads to earlier onset potentials; (b) but (tpfc)Mo^V(O) is more active (higher k_{obs} and i_{cat}/i_p values) toward proton reduction compared to (tpfc-Br$_8$)Mo^V(O) and (tfc)Mo^V(O); and (c) the differences in catalytic efficacy may further be appreciated by comparing the maximal currents obtained in the presence of 6 equivalents acid at voltages that are identical to the Mo^{III}/Mo^{IV} redox potential of each complex: 156 μA at −1.46 V for (tpfc)Mo^V(O), 85 μA at −1.22 V for (tfc)Mo^V(O), and 2 μA at −0.82 V for (tpfc-Br$_8$)Mo^V(O) (Table S2).

Chronoamperometric experiments accompanied with gas chromatographic analysis for quantification of hydrogen gas generation were performed for providing confidence regarding the catalytic process, as well as for confirming the above conclusions and possibly gaining additional information about the operating mechanisms. Bulk electrolysis was carried out in a 0.1M TBAP/DMF solution containing 0.04 mM catalyst and large excess of acid (4 mM), under a constant potential of −2.1 V for 1 hr. Bubbles started to appear on the working glassy carbon electrode surface after about 20 min (Figure S16); and the formation of H_2 during electrolysis was quantified by gas chromatography (GC) analysis of a known volume from the head space of the electrolysis cell. The calculation of Faradaic efficiency (FE) was done by subtraction of hydrogen formation in blank experiments (under the same electrochemical condition but without catalyst) (Figure S16). An excellent FE of 96% was determined in the case of (tpfc)Mo^V(O), much larger than for (tfc)Mo^V(O) (56%) and (tpfc-Br$_8$)Mo^V(O) (26%). Besides being the most active catalyst toward proton reduction, (tpfc)Mo^V(O) appeared also to be the most stable complex according to UV-vis measurements after bulk electrolysis (Figures S17–S19). The UV-vis spectra of both (tpfc-Br$_8$)Mo^V(O) and (tfc)Mo^V(O) displayed signs indicative of decomposition: decrease in the Soret band and considerable increase in the base line, respectively.

The results obtained within this series of (oxo)molybdenum corroles served well for deducing some limited mechanism of action information regarding HER catalysis thereby. All complexes display two reversible processes in the absence of acid (Figure 2), thus testifying that the (oxo)molybdenum moiety remains intact upon reduction (Scheme 1). This statement is true for the 1-electron reduced complexes even in the presence of acid (Figures 3 and 4), i.e., the negatively charged (oxo)Mo(IV) corroles are evidently inert to acid. This is consistent with the molecular orbital description of the terminal Mo-O bond therein: while reduction of the complex changes it from neutral to anionic, the bond order (one sigma and two p bonds,

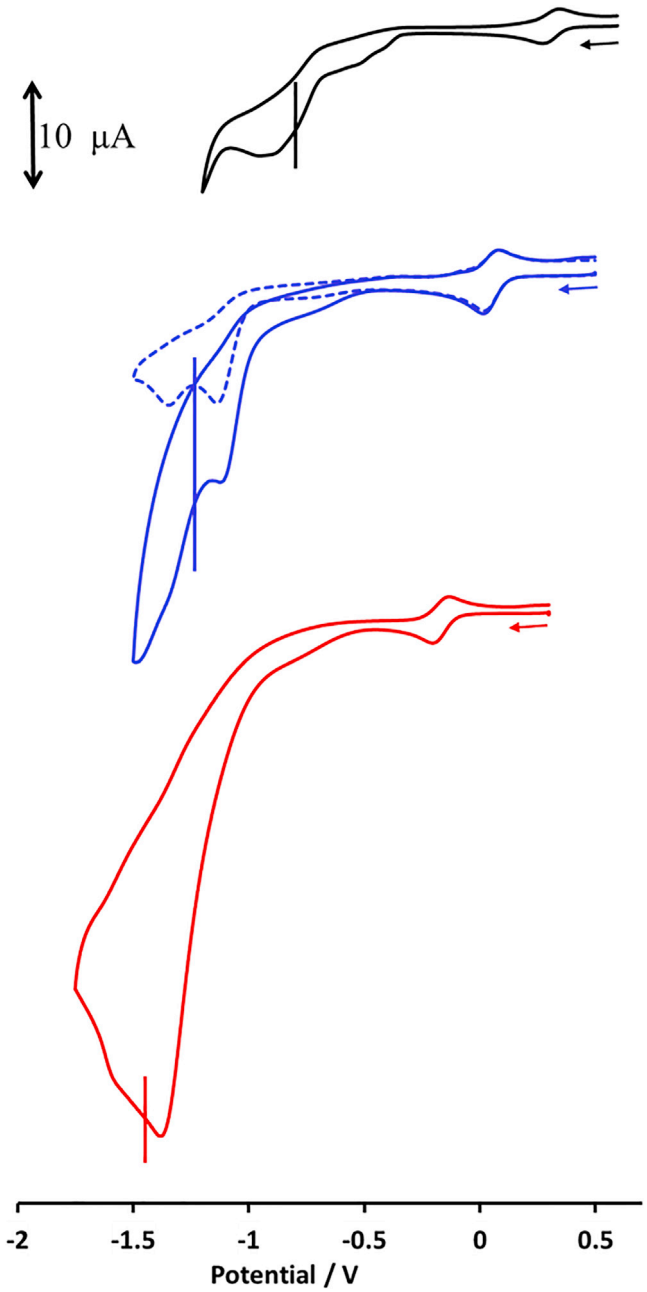

Figure 4. The influence of DMF-H$^+$ on cyclic voltammograms of (oxo)molybdenum(V) corroles

Comparison of the cyclic voltammograms obtained in the presence of DMF-H$^+$ (29 equiv., dashed line with 6 equiv.) for (tpfc)Mo^V(O), (red trace), (tpfc-Br$_8$)Mo^V(O), (black trace), and (tfc)MO^V(O) (solid and dashed blue traces). The vertical lines show the [Mo(O)]$^{2-}$/[Mo(O)]$^-$ redox potential in the absence of acid. Catalyst concentration = 1 mM.

all 2 center-2 electrons) and the oxygen to metal π back donations are not and hardly affected, respectively. On the other hand, further reduction to d^3 molybdenum(III) reduces the bond order from 3 to 2 and turns the oxygen atom to be much more basic because π back donation to the metal becomes much less effective. The electrocatalytic process may start at less negative voltages than the redox potentials in the absence of acid when (even partial) protonation occurs either before or during reduction (the well-known PCET process) (Weinberg et al., 2012). The catalytic current for catalysis by (tpfc)Mo(O) (Figure 3) increases linearly with acid concentration, thus pointing toward a 1e$^-$/2H$^+$ process that leads to neutral molybdenum(III) (Scheme 1, left); and the same holds true for the more prominent catalytic waves of (tfc)Mo(O)

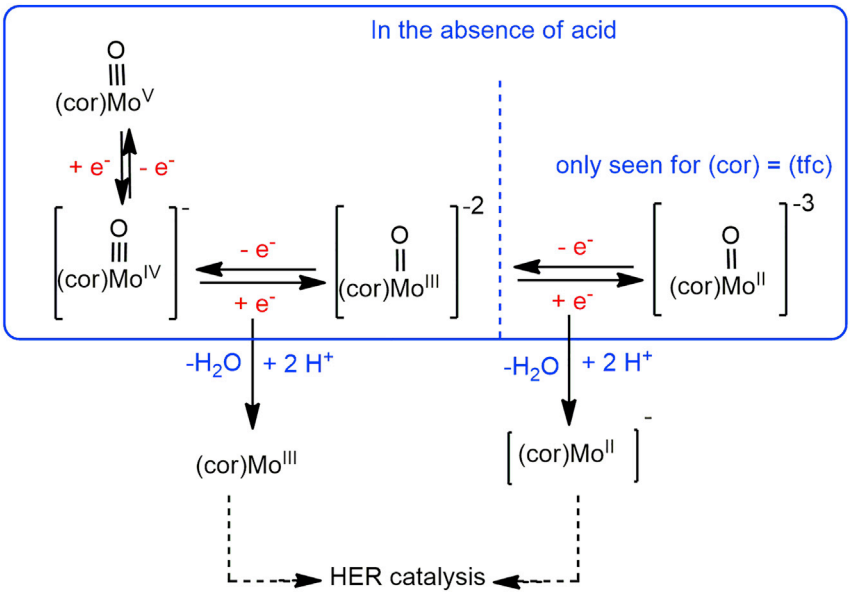

Scheme 1. The redox processes of the (oxo)molybdenum(V) corrole complexes in the absence and presence of acid
Note that the doubly reduced complexes are not only more basic but also of reduced (double rather than triple) metal-oxygen bond order. (cor = tranionic corrolato).

(Figures 4 and S12). In the latter case, this takes place later than the (oxo)Mo^{IV}/(oxo)Mo^{III} redox couple, thus suggesting that the charged molybdenum(II) is formed (Scheme 1, right).

Heterogeneous HER electrocatalysis

Keeping in mind that the ultimate goal is HER catalysis in aqueous environment, (tfc)Mo^{V}(O) and (tpfc)Mo^{V}(O) were adsorbed on Vulcan XC72R carbon by adding the latter to isopropanol solutions of the former (Figure S20). The adsorbed amounts of the catalysts were calculated by comparing the UV-Vis spectra of their original solutions before and after the addition of the carbon, revealing it to be 72% for (tfc)Mo^{V}(O) and 68% for (tpfc)Mo^{V}(O). But considering the molecular weight differences between the two complexes, the (moles of catalyst)/carbon ratio is actually about 60% larger for (tfc)Mo^{V}(O) than for (tpfc)Mo^{V}(O). The modified carbons were adsorbed on the surface of glassy carbon electrodes for testing their performance for electrocatalytic proton reduction of acidic water. The recorded cyclic voltammograms (Figure 5A) uncovered (a) more than 2 orders of magnitude larger currents than under homogeneous conditions; (b) larger current and earlier catalytic onset for the electrode modified by (tfc)Mo(O); (c) an electric charge curve (during 10 hr of bulk electrolysis!) that is more ideal (almost no curvature) for the latter, thus testifying for its larger durability; and (d) an only 280 mV difference in onset potential relative to 20% Pt on carbon, which ranks (tfc)Mo(O) among the best non-precious-metal HER catalysts (Zeng and Li, 2015). Upon the application of negative potentials on the modified electrodes immersed in 0.5 M sulfuric acid solutions, hydrogen bubbles generated on the electrode's surface were clearly visible (Figure 5B). Quantification of the thus generated hydrogen gas was performed by headspace gas chromatographic analysis. At −0.8 V (vs. Ag/AgCl), (tfc)Mo^{V}(O) and (tpfc)Mo^{V}(O) were found to be very effective catalysts for proton reduction with a FE of 97% and 80%, respectively.

Conclusions

We provide fresh insight into the chemistry of molybdenum corroles, achieved via the introduction of new and fully characterized complexes wherein the (oxo)molybdenum(V) moiety is chelated by derivatives with electron withdrawing substituents. Although substituents on the corrole periphery affect mainly its π system, the metal-centered reductions still differ by more than 0.67 V within this series. The basicity of the terminal metal-oxo bond toward the very strong DMF-H^+ acid is extremely low and comes into play only for the doubly reduced complexes and mostly so for the one chelated by the least electron withdrawing corrole. That complex completes a catalytic cycle for the reduction of protons to hydrogen gas, via coinciding proton- and electron-transfer processes, at a voltage that is lower than its Mo(III)/Mo(IV) reduction potential

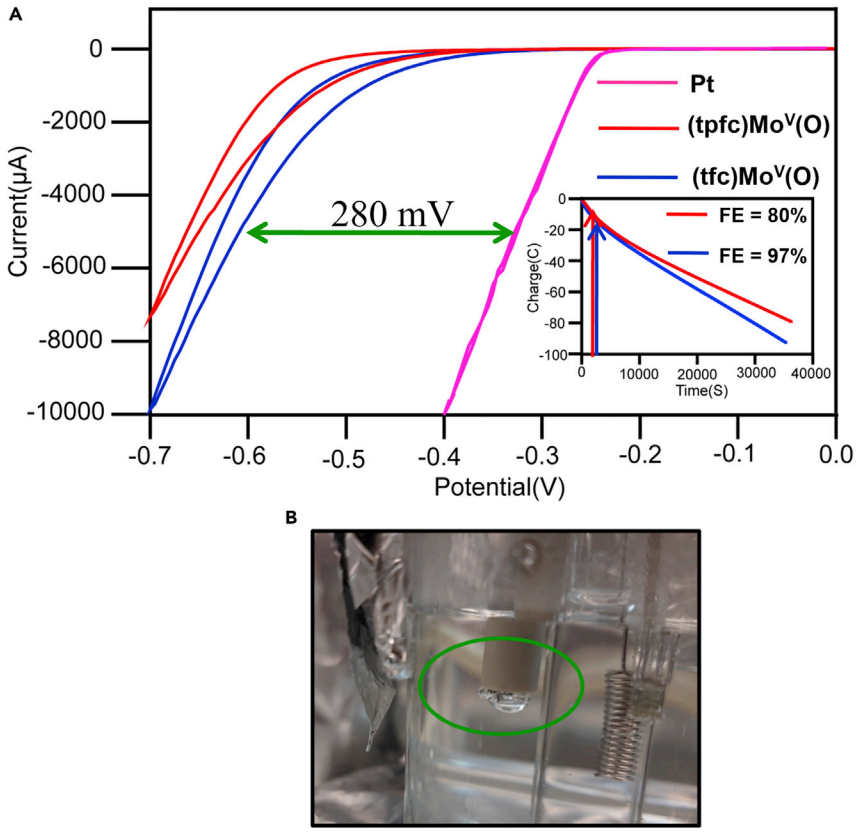

Figure 5. The performance of (oxo)molybdenum(V) corroles for H_2 generation under heterogeneous conditions

(A) Comparison between the cyclic voltammograms of (tfc)Mo(O) and (tpfc)Mo(O) adsorbed onto Vulcan XC72R carbon as the solid support, in N_2-saturated 0.5 M H_2SO_4 solution, in comparison with 20% Pt adsorbed onto Vulcan XC72R carbon under the same conditions. Scan rate: 50 mV/s, reference electrode: Ag/AgCl. Inset: electric charge curves during 10 hr of bulk electrolysis at applied potential of −0.8 V.

(B) View of H_2 generation in the form of bubbles on the surface of a glassy carbon electrode that was modified by (tfc)Mo(O), after 10 min of bulk electrolysis; applied potential −0.8 V vs. Ag/AgCl.

in the absence of acid. That pathway is less effective for the complexes wherein the corrole substituents reduce the basicity of the N4 coordination core and consequentially that of the molybdenum-bound oxygen atom as well. (tpfc)Mo^V(O) is the most active homogeneous electrocatalyst for HER in organic solvent, but the (tfc)Mo^V(O)-modified electrode performs best for hydrogen gas generation from acidic water in terms of early onset potential, FE, and durability. We anticipate that disclosure of the utility of stable oxo-metal complexes as electrocatalyst for hydrogen production from protons will raise the interest in using them for even more demanding reduction processes.

Limitations of the study

Isolation of the proposed molybdenum(III) corrole reaction intermediate was not yet achieved; and future research that will focus on the catalyst-modified electrodes is required.

STAR★METHODS

Detailed methods are provided in the online version of this paper and include the following:

- KEY RESOURCES TABLE
- RESOURCES AVAILABILITY
  - Lead contact
  - Materials availability
  - Data and code availability
- METHOD DETAILS

SUPPLEMENTAL INFORMATION

Supplemental information can be found online at https://doi.org/10.1016/j.isci.2021.102924.

ACKNOWLEDGMENTS

This article is dedicated in beloved memory of late I.G. (13.06.1945 to 18.02.2018) and with great admiration for his seminal contributions to the science of crystallography in general and of porphyrins and corroles in particular. Financial support of this research by the PAZY Foundation to Z.G. and A. Mizrahi is highly appreciated.

AUTHOR CONTRIBUTIONS

P.Y. and I.N.-E. synthesized the molybdenum corroles and performed the homogeneous electrocatalysis. A.K. executed the heterogeneous electrocatalysis. A. Mizrahi measured the cyclic voltammograms. A. Mahammed designed the experiments and wrote the paper. N.F., S.L., and I.G. did the X-ray crystallographic measurements. Z.G. designed the experiments and wrote the paper.

DECLARATION OF INTERESTS

The authors declare no competing interests.

Received: May 10, 2021
Revised: June 28, 2021
Accepted: July 26, 2021
Published: August 20, 2021

SUPPORTING CITATIONS

The following reference appears in the supplemental information (Bourhis et al., 2015; Dolomanov et al., 2009; Hooft, 1999; Mahammed et al., 2011; Otwinowski and Minor, 1997; Yadav et al., 2020).

REFERENCES

Abbas, M.A., and Bang, J.H. (2015). Rising again: opportunities and challenges for platinum-free electrocatalysts. Chem. Mater. *27*, 7218–7235. https://doi.org/10.1021/acs.chemmater.5b03331.

Alemayehu, A.B., Vazquez-Lima, H., McCormick, L.J., and Ghosh, A. (2017). Relativistic effects in metallocorroles: comparison of molybdenum and tungsten biscorroles. Chem. Commun. *53*, 5830–5833. https://doi.org/10.1039/C7CC01549F.

Benck, J.D., Hellstern, T.R., Kibsgaard, J., Chakthranont, P., and Jaramillo, T.F. (2014). Catalyzing the hydrogen evolution reaction (HER) with molybdenum sulfide nanomaterials. ACS Catal. *4*, 3957–3971. https://doi.org/10.1021/cs500923c.

Bhyrappa, P., Purushothaman, B., and Vittal, J.J. (2003). Highly brominated porphyrins: synthesis, structure and their properties. J. Porphyr. Phthalocyanines *07*, 682–692. https://doi.org/10.1142/s1088424603000859.

Bourhis, L.J., Dolomanov, O.V., Gildea, R.J., Howard, J.A.K., and Puschmann, H. (2015). The anatomy of a comprehensive constrained, restrained refinement program for the modern computing environment - olex2 dissected. Acta Crys. Sec. A *71*, 59–75. https://doi.org/10.1107/S2053273314022207.

Buckley, H.L., and Arnold, J. (2015). Recent developments in out-of-plane metallocorrole chemistry across the periodic table. Dalton. Trans. *44*, 30–36. https://doi.org/10.1039/C4DT02277G.

Bullock, R.M., Appel, A.M., and Helm, M.L. (2014). Production of hydrogen by electrocatalysis: making the H–H bond by combining protons and hydrides. Chem. Commun. *50*, 3125–3143. https://doi.org/10.1039/C3CC46135A.

Carrasco, C.J., Montilla, F., and Galindo, A. (2018). Molybdenum-catalyzed enantioselective sulfoxidation controlled by a nonclassical hydrogen bond between coordinated chiral imidazolium-based dicarboxylate and peroxido ligands. Molecules *23*, 1595.

Chatzistathis, T. (2014). Molybdenum deficiency. In Micronutrient Deficiency in Soils and Plants, T. Chatzistathis, ed. (Bentham Science), pp. 157–171.

Chen, Q.-C., Soll, M., Mizrahi, A., Saltsman, I., Fridman, N., Saphier, M., and Gross, Z. (2018). One-pot synthesis of contracted and expanded porphyrins with meso-CF3 groups. Angew. Chem. Int. Ed. *57*, 1006–1010. https://doi.org/10.1002/anie.201710106.

Chen, Y., Fan, Q.-H., Hossain, M.S., Zhan, S.-Z., Liu, H.-Y., and Si, L.-P. (2020). Electrocatalytic hydrogen evolution of cobalt and free-base triaryl corrole bearing hydroxyethyl amino groups. Eur. J. Inorg. Chem. *2020*, 491–498. https://doi.org/10.1002/ejic.201900996.

Dolomanov, O.V., Bourhis, L.J., Gildea, R.J., Howard, J.A.K., and Puschmann, H. (2009). OLEX2: a complete structure solution, refinement and analysis program. J. Appl. Cryst. *42*, 339–341. https://doi.org/10.1107/S0021889808042726.

Fukuzumi, S., Lee, Y.-M., and Nam, W. (2018). Thermal and photocatalytic production of hydrogen with earth-abundant metal complexes. Coord. Chem. Rev. *355*, 54–73. https://doi.org/10.1016/j.ccr.2017.07.014.

Golubkov, G., Bendix, J., Gray, H.B., Mahammed, A., Goldberg, I., DiBilio, A.J., and Gross, Z. (2001). High-valent manganese corroles and the first perhalogenated metallocorrole catalyst. Angew. Chem. Int. Ed. *40*, 2132–2134. https://doi.org/10.1002/1521-3773(20010601)40:11<2132::AID-ANIE2132>3.0.CO;2-5.

Gross, Z., Golubkov, G., and Simkhovich, L. (2000). Epoxidation catalysis by a manganese corrole and isolation of an oxomanganese(V) corrole. Angew. Chem. Int. Ed. *39*, 4045–4047. https://doi.org/10.1002/1521-3773(20001117)39:22<4045::AID-ANIE4045>3.0.CO;2-P.

Guo, X., Wang, N., Li, X., Zhang, Z., Zhao, J., Ren, W., Ding, S., Xu, G., Li, J., Apfel, U.-P., et al. (2020). Homolytic versus heterolytic hydrogen evolution reaction steered by a steric effect. Angew. Chem. Int. Ed. *59*, 8941–8946. https://doi.org/10.1002/anie.202002311.

Hooft, R. (1999). KappaCCD Collect Software (Nonius BV).

Hua, W., Sun, H.-H., Xu, F., and Wang, J.-G. (2020). A review and perspective on molybdenum-based electrocatalysts for hydrogen evolution reaction. Rare Met. *39*, 335–351. https://doi.org/10.1007/s12598-020-01384-7.

Johansen, I., Norheim, H.-K., Larsen, S., Alemayehu, A.B., Conradie, J., and Ghosh, A. (2011). Substituent effects on metallocorrole spectra: insights from chromium-oxo and molybdenum-oxo triarylcorroles. J. Porphyrins Phthalocyanines *15*, 1335–1344. https://doi.org/10.1142/s1088424611004270.

Lei, H., Fang, H., Han, Y., Lai, W., Fu, X., and Cao, R. (2015). Reactivity and mechanism studies of hydrogen evolution catalyzed by copper corroles. ACS Catal. *5*, 5145–5153. https://doi.org/10.1021/acscatal.5b00666.

Lei, H., Han, A., Li, F., Zhang, M., Han, Y., Du, P., Lai, W., and Cao, R. (2014). Electrochemical, spectroscopic and theoretical studies of a simple bifunctional cobalt corrole catalyst for oxygen evolution and hydrogen production. Phys. Chem. Chem. Phys. *16*, 1883–1893. https://doi.org/10.1039/C3CP54361G.

Lin, H., Hossain, M.S., Zhan, S.-Z., Liu, H.-Y., and Si, L.-P. (2020). Electrocatalytic hydrogen evolution using triaryl corrole cobalt complex. Appl. Organomet. Chem. *34*, e5583. https://doi.org/10.1002/aoc.5583.

Luobeznova, I., Raizman, M., Goldberg, I., and Gross, Z. (2006). Synthesis and full characterization of molybdenum and antimony corroles and utilization of the latter complexes as very efficient catalysts for highly selective aerobic oxygenation reactions. Inorg. Chem. *45*, 386–394. https://doi.org/10.1021/ic051483g.

Mahammed, A., Botoshansky, M., and Gross, Z. (2012). Chlorinated corroles. Dalton Trans. *41*, 10938–10940. https://doi.org/10.1039/C2DT31261A.

Mahammed, A., Mondal, B., Rana, A., Dey, A., and Gross, Z. (2014). The cobalt corrole catalyzed hydrogen evolution reaction: surprising electronic effects and characterization of key reaction intermediates. Chem. Commun. *50*, 2725–2727. https://doi.org/10.1039/C3CC48462A.

Mahammed, A., Tumanskii, B., and Gross, Z. (2011). Effect of bromination on the electrochemistry, frontier orbitals, and spectroscopy of metallocorroles. J. Porphyr. Phthalocyanines *15*, 1275–1286. https://doi.org/10.1142/s1088424611004191.

Mandoj, F., Nardis, S., Pomarico, G., and Paolesse, R. (2008). Demetalation of corrole complexes: an old dream turning into reality. J. Porphyr. Phthalocyanines *12*, 19–26. https://doi.org/10.1142/s1088424608000042.

Mody, V.V., Fitzpatrick, M.B., Zabaneh, S.S., Czernuszewicz, R.S., Gałęzowski, M., and Gryko, D.T. (2009). Solvent effects on the electronic and vibrational properties of high-valent oxomolybdenum(V) 5,10,15-triphenylcorrole probed by UV-visible and resonance Raman spectroscopy. J. Porphyrins Phthalocyanines *13*, 1040–1052. https://doi.org/10.1142/s1088424609001364.

Mondal, B., Sengupta, K., Rana, A., Mahammed, A., Botoshansky, M., Dey, S.G., Gross, Z., and Dey, A. (2013). Cobalt corrole catalyst for efficient hydrogen evolution reaction from H2O under ambient conditions: reactivity, spectroscopy, and density functional theory calculations. Inorg. Chem. *52*, 3381–3387. https://doi.org/10.1021/ic4000473.

Nayak, M., Nayak, P., Sahu, K., and Kar, S. (2020). Synthesis, characterization, and application of oxo-molybdenum(V)-Corrolato complexes in epoxidation reactions. J. Org. Chem. *85*, 11654–11662. https://doi.org/10.1021/acs.joc.0c01146.

Nigel-Etinger, I., Goldberg, I., and Gross, Z. (2013). Intriguing chemistry of molybdenum corroles. Inorg. Chem. *52*, 4139–4141. https://doi.org/10.1021/ic400116u.

Otwinowski, Z., and Minor, W. (1997). Processing of X-ray diffraction data collected in oscillation mode. Methods Enzymol. *276*, 307–326.

Roger, I., Shipman, M.A., and Symes, M.D. (2017). Earth-abundant catalysts for electrochemical and photoelectrochemical water splitting. Nat. Rev. Chem. *1*, 0003. https://doi.org/10.1038/s41570-016-0003.

Sashuk, V., Koszarna, B., Winiarek, P., Gryko, D.T., and Grela, K. (2004). The simple synthesis of sh A3- and trans-A2B-molybdenum(V) corrolates. Inorg. Chem. Commun. *7*, 871–875. https://doi.org/10.1016/j.inoche.2004.05.010.

Schwarz, G., Mendel, R.R., and Ribbe, M.W. (2009). Molybdenum cofactors, enzymes and pathways. Nature *460*, 839–847. https://doi.org/10.1038/nature08302.

Schweyen, P., Brandhorst, K., Hoffmann, M., Wolfram, B., Zaretzke, M.-K., and Bröring, M. (2017). Viking helmet corroles: activating inert oxidometal corroles. Chem. A. Eur. J. *23*, 13897–13900. https://doi.org/10.1002/chem.201703721.

Spence, J.T. (1980). Chapter 3 - model reactions of molybdenum complexes. In Molybdenum and Molybdenum-Containing Enzymes, M.P. Coughlan, ed. (Pergamon), pp. 99–118.

Sudhakar, K., Mahammed, A., Chen, Q.-C., Fridman, N., Tumanskii, B., and Gross, Z. (2020). Copper complexes of CF3-substituted corroles for affecting redox potentials and electrocatalysis. ACS Appl. Energy Mater. *3*, 2828–2836. https://doi.org/10.1021/acsaem.9b02465.

Sudhakar, K., Mizrahi, A., Kosa, M., Fridman, N., Tumanskii, B., Saphier, M., and Gross, Z. (2017). Effect of selective CF3 substitution on the physical and chemical properties of gold corroles. Angew. Chem. Int. Ed. *56*, 9837–9841. https://doi.org/10.1002/anie.201705007.

Sun, H., Han, Y., Lei, H., Chen, M., and Cao, R. (2017). Cobalt corroles with phosphonic acid pendants as catalysts for oxygen and hydrogen evolution from neutral aqueous solution. Chem. Commun. *53*, 6195–6198. https://doi.org/10.1039/c7cc02400b.

Thiruvengetam, P., and Chand, D.K. (2018). Oxidomolybdenum based catalysts for sulfoxidation reactions: a brief Review. J. Indian Chem. Soc. *95*, 781–788.

Weare, W.W., Dai, X., Byrnes, M.J., Chin, J.M., Schrock, R.R., and Müller, P. (2006). Catalytic reduction of dinitrogen to ammonia at a single molybdenum center. Proc. Natl. Acad. Sci. U S A *103*, 17099–17106. https://doi.org/10.1073/pnas.0602778103.

Weinberg, D.R., Gagliardi, C.J., Hull, J.F., Murphy, C.F., Kent, C.A., Westlake, B.C., Paul, A., Ess, D.H., McCafferty, D.G., and Meyer, T.J. (2012). Proton-coupled electron transfer. Chem. Rev. *112*, 4016–4093. https://doi.org/10.1021/cr200177j.

Wickramasinghe, L.A., Ogawa, T., Schrock, R.R., and Müller, P. (2017). Reduction of dinitrogen to ammonia catalyzed by molybdenum diamido complexes. J. Am. Chem. Soc. *139*, 9132–9135. https://doi.org/10.1021/jacs.7b04800.

Xiao, P., Sk, M.A., Thia, L., Ge, X., Lim, R.J., Wang, J.-Y., Lim, K.H., and Wang, X. (2014). Molybdenum phosphide as an efficient electrocatalyst for the hydrogen evolution reaction. Energ. Environ. Sci. *7*, 2624–2629. https://doi.org/10.1039/C4EE00957F.

Xie, L., Tian, J., Ouyang, Y., Guo, X., Zhang, W., Apfel, U.-P., Zhang, W., and Cao, R. (2020). Water-soluble polymers with appending porphyrins as bioinspired catalysts for the hydrogen evolution reaction. Angew. Chem. Int. Ed. *59*, 15844–15848. https://doi.org/10.1002/anie.202003836.

Yadav, P., Khoury, S., Mahammed, A., Morales, M., Virgil, S.C., Gray, H.B., and Gross, Z. (2020). Enhanced synthetic access to tris-CF3-substituted corroles. Org. Lett. *22*, 3119–3122. https://doi.org/10.1021/acs.orglett.0c00879.

Zeng, M., and Li, Y. (2015). Recent advances in heterogeneous electrocatalysts for the hydrogen evolution reaction. J. Mater. Chem. A *3*, 14942–14962. https://doi.org/10.1039/C5TA02974K.

Zhong, Y.-Q., Hossain, M.S., Chen, Y., Fan, Q.-H., Zhan, S.-Z., and Liu, H.-Y. (2019). A comparative study of electrocatalytic hydrogen evolution by iron complexes of corrole and porphyrin from acetic acid and water. Transit. Met. Chem. *44*, 399–406. https://doi.org/10.1007/s11243-019-00307-5.

STAR★METHODS

KEY RESOURCES TABLE

REAGENT or RESOURCE	SOURCE	IDENTIFIER
Chemicals		
$Mo(CO)_6$	MERCK	Cat# 8003960010 CAS: 13939-06-5
Nafion	MERCK	Cat# 274704 CAS: 31175-20-9
20% Pt on Vulcan XC72	Premetek.com	Item # P10A200

RESOURCES AVAILABILITY

Lead contact

Further information and requests for resources and reagents should be directed to and will be fulfilled by the lead contact, Zeev Gross (chr10zg@technion.ac.il).

Materials availability

This study did not generate new unique reagents.

Data and code availability

- All data reported in this paper will be shared by the lead contact upon request.
- This paper dose not report original code.
- Any additional information required to analyze the data reported in this paper is available from the lead contact upon request.

METHOD DETAILS

^{1}H and ^{19}F NMR spectra were recorded on Bruker Avance 200 spectrometer (200 MHz for ^{1}H and 188 MHz for ^{19}F). Chemical shifts are reported in ppm relative to the residual proton resonances in deuterated solvents, and relative to $CFCl_3$ in the ^{19}F NMR spectra. Mass spectra were recorded on Brucker maXis impact using APCI positive method. Absorption spectra were recorded using an Agilent Cary 8454 UV-visible spectrophotometer.

The electrochemical measurements were recorded using a conventional three electrode system consisting of a glassy carbon working electrode (diameter of the active zone: 2.8 mm; Metrohm), a platinum wire as counter electrode and Ag/AgCl reference electrode in DMF using 1 mM catalyst and 0.1 M TBAP electrolyte. Electrochemical measurements were recorded with an EmStat3+ electrochemical system (Fc/Fc^{+} couple = 0.529 V vs. Ag/AgCl). Bulk electrolysis was carried out in 100 mL cell with a glassy carbon working electrode and a Pt wire counter electrode. H_2 gas was collected by gas-tight syringes from the head space after electrolysis and quantified by a Sion GC-TCD detector using HP-mole sieve column and N_2 as a carrier gas. The volume of H_2 produced by $Mo^{V}(O)$ corroles was calculated by using a calibration curve vs. known volumes of H_2 gas. The catalysis was run from the same batch which the crystals for XRD were obtained.

The single-crystal material was immersed in Paratone–N oil and mounted on APEX II Bruker diffractometer at low temperature. Data collection was performed using monochromated Mo Kα radiation, λ = 0.71073 Å, using ϕ and ω scans to cover the Ewald sphere (Hooft, 1999). Accurate cell parameters were obtained with the amount of indicated reflections (Otwinowski and Minor, 1997). Using Olex2, the structure was solved with the olex2.solve structure solution program using Charge Flipping and refined with the ShelXL refinement package using Least Squares minimization (Bourhis et al., 2015; Dolomanov et al., 2009). Software used for molecular graphics was Mercury 3.5. Crystallographic data for $(tpfc\text{-}Cl_6)Mo^{V}(O)$, $(tpfc\text{-}Br_8)Mo^{V}(O)$ and $(tfc)Mo^{V}(O)$ have been deposited in the Cambridge Crystallographic Data Center (CCDC)

under accession numbers CCDC 2038755, 2038745 and 2036935, respectively. These data can be obtained free of charge from the CCDC at http://www.ccdc.cam.ac.uk/data_request/cif.

(tpfc)Mo^{V}(O) was prepared as reported earlier (Luobeznova et al., 2006).

A solution of H_3(tpfc)Br_8 (Mahammed et al., 2011) (50 mg, 0.03 mmol) in decalin (50 mL) was heated to 170-180°C, followed by the addition of [(cyclopentadienyl)Mo^{V} tetrachloride], (50 mg, 0.17 mmol). TLC examinations (silica gel, n-hexane/ethyl-acetate) 2:1) revealed that the starting material was fully consumed within 40 minutes of reaction, after which the solvents were evaporated. Column chromatography on silica gel 60 (eluent: starting with hexane/ethyl-acetate 2:1 and gradually changing to ethyl acetate only) was applied for cleaning the polar product. Crystallization from a THF/n-heptane mixture afforded (tpfc)Mo^{V}(O) Br_8 as green-red solid in 87% yield (40 mg, 0.026 mmol,).^{19}F-NMR (THF-d_8): δ, ppm -138.3 (br d, 4F), -153.2 (br s, 2F), -164.5 (br s, 4F). UV-vis (CH_2Cl_2, λ_{max} (ε, $M^{-1}cm^{-1}$)): 450 (69,000), 556 (3,600), 598 (10,600) nm. HRMS (ACPI, positive mode) for $C_{37}Br_8F_{15}N_4MoO$ (M^+): *m/z* = 1530.2354 (calculated) 1530.2232 (observed).

A solution of H_3(tfc) (Yadav et al., 2020) (20 mg, 0.04 mmol) in decalin (10 mL) was heated to 170-180 °C, followed by the addition of $Mo(CO)_6$ (105 mg, 0.40 mmol). TLC examinations (silica gel, *n*-hexane/CH_2Cl_2 3:1) revealed that the starting material was fully consumed within 1 h of reaction. The reaction mixture was directly loaded over silica gel, 100 % *n*-hexane was used as eluent to remove decalin, after which MoTFC was eluted as a red fraction by using 3:1 *n*-hexane/CH_2Cl_2 mixtures. Solvent evaporation and crystallization from a $CHCl_3$/*n*-hexane mixture yielded 10 mg (0.016 mmol, 40% yield) of (tfc)Mo(O). UV-vis (CH_2Cl_2, λ_{max} (ε, $M^{-1}cm^{-1}$)): 429 (65,500), 546 (6,500), 582 (10,800) nm. HRMS (ACPI, positive mode) for $C_{22}H_8F_9N_4MoO$ (M^+): *m/z* = 612.9608 (calculated) 612.9608 (observed).

The corroles (0.8 mg) (tfc)Mo(O) and (tpfc)Mo(O) were dissolved in isopropanol (1 mL) and Vulcan XC72R carbon (10 mg of) was added. The suspension was sonicated for 20 min and stirred overnight at room temperature, after which the corrole-adsorbed carbon nanoparticles were separated by centrifugation. Electronic spectra examinations of the isopropanol solutions before and after that treatment were used for calculating the amount of corrole that was adsorbed on the carbon (Figure S18). The modified carbons were dried overnight 45 °C, 1 mL isopropanol was added and after another overnight stirring followed by centrifugation, they were dried again overnight at 45 °C. Inks of corrole-containing carbon were prepared by mixing 1 mg amounts with 0.2 mL isopropanol, 0.8 mL H_2O, and 10 μL of Nafion, followed by 20 min sonication. Fresh amounts of such prepared inks were adsorbed on the surface of glassy carbon electrodes (diameter of the carbon surface: 2.8 mm; Metrohm), by dropping 5 μl on the GC electrode and drying for 40 min at 45°C. This procedure was repeated twice.